msp

Algebraic & Geometric Topology 14 (2014) 1307–1337

An alternative approach to hyperbolic structures on link complements

MORWEN THISTLETHWAITE
ANASTASIIA TSVIETKOVA

An alternative method is described for determining the hyperbolic structure on a link complement, and some of its elementary consequences are examined. The method is particularly suited to alternating links.

57M25, 57M50

1 Overview

The purpose of this article is to describe an alternative method for calculating the hyperbolic structure on a classical link complement. The method does not use an ideal triangulation of the complement, but instead considers the shapes of ideal polygons bounding the regions of a diagram of the link. In order to guarantee the applicability of our method, we shall impose a "minimality" condition on the checkerboard surfaces of our link diagrams:

Definition 1.1 A diagram of a hyperbolic link is *taut* if each associated checkerboard surface is incompressible and boundary incompressible in the link complement, and moreover does not contain any simple closed curve representing an accidental parabolic.

From this definition it follows that if α is a proper, non-separating arc in a checkerboard surface associated to a taut diagram, and $\widetilde{\alpha}$ is a lift of α to the universal cover $\mathbb{H}^3$, then the ends of $\widetilde{\alpha}$ are at the centres of distinct horoballs; thus α is properly homotopic to a geodesic. In particular, at each crossing of the diagram, the arc travelling vertically from underpass to overpass, ie a "polar axis" in the terminology of Menasco [13], gives rise in this manner to a geodesic; such geodesics, henceforth called *crossing geodesics*, will form the edges of the ideal polygons mentioned above.

Although the method is applicable to any taut link diagram, we are particularly interested in applying it to hyperbolic alternating links, as the resulting hyperbolicity equations assume a reasonably pleasing form. We recall that it is proved in [13] that prime

Published: 7 April 2014 DOI: 10.2140/agt.2014.14.1307

alternating link complements cannot contain essential tori, and since the only alternating torus links are those of type $(2,n)$, it follows from W Thurston's hyperbolization theorem that an alternating link is hyperbolic if and only if it is prime and is not a $(2,n)$–torus link. From [13] a reduced alternating link diagram represents a prime link if and only if it is prime in the diagrammatic sense, and from Menasco and Thistlethwaite [14] each reduced alternating diagram of a $(2,n)$–torus link is standard; therefore one can tell by inspection whether a link presented as a reduced alternating diagram is hyperbolic.

Proposition 1.2 *Each reduced alternating diagram of a hyperbolic alternating link is taut.*

Proof It is proved in [14] that the checkerboard surfaces for such link diagrams are incompressible and boundary incompressible, and it is proved in Adams [3], and Futer, Kalfagianni and Purcell [10] that they are quasi-Fuchsian, hence contain no accidental parabolics. □

Note 1.3 In [10], the authors state their results for a more general class of diagrams than alternating. However, the spanning surfaces considered are so-called *state surfaces*; for non-alternating diagrams these are different from checkerboard surfaces, and we do not know at present whether these can be incorporated into our method of computing hyperbolic structures.

It would be interesting to know whether there exists a hyperbolic link not admitting a taut diagram.

2 The geometry of an ideal polygon

Let F be a checkerboard surface for a connected diagram D of a link L. Then F is the union of disks, one for each region coloured, say, black in the checkerboard colouring of the diagram. The boundary of each disk is an alternating sequence of (i) sub-arcs of the link travelling between adjacent crossings incident to the region, and (ii) "polar axis" arcs travelling between the underpass and the overpass at a crossing. The disks are glued together along the polar axis arcs.

Now suppose that D is taut; let R be a black region of D with $n \geq 2$ sides, and let $\Delta_R \subset F$ be the associated disk. Then $\Delta_R - L$ is homeomorphic to a disk with n points of its boundary removed, which we may describe as a "filled-in ideal n–gon"; this lifts homeomorphically to a filled-in ideal n–gon $\widetilde{\Delta_R}$ in the upper half-space model

of $\mathbb{H}^3$. The n ideal vertices of $\widetilde{\Delta_R}$ correspond to the n arcs of $\Delta_R \cap L$ (which in turn correspond to edges of the region R), and the edges of the ideal n–gon boundary of $\widetilde{\Delta_R}$ are lifts of the interiors of the n polar axis arcs in $\partial\Delta_R$.

In order to proceed further, we need to show that $\widetilde{\Delta_R}$ satisfies a non-degeneracy condition.

Proposition 2.1 *The n ideal vertices of $\widetilde{\Delta_R}$ are pairwise distinct.*

Proof Let α_1, α_2 be any two arc components of $\Delta_R \cap L$, and let γ be an arc properly embedded in Δ_R that travels from a point of α_1 to a point of α_2. Then the interior of γ lifts to an arc in $\widetilde{\Delta_R}$ travelling between the corresponding ideal vertices. Since the link diagram is taut and γ is non-separating in the checkerboard surface F, the conclusion follows. □

As usual, we identify the boundary of $\mathbb{H}^3$ with the Riemann sphere $\mathbb{C} \cup \{\infty\}$. Let R be a region of the link diagram with at least three sides, and let the ideal vertices of $\widetilde{\Delta_R}$ be $z_1, \dots, z_n$ in cyclic order; then, from Proposition 2.1, these n points define an ideal n–gon $\widetilde{\Pi_R}$ in $\mathbb{H}^3$, with geodesic edges that are pairwise distinct.

Let γ_i be the geodesic edge of $\widetilde{\Pi_R}$ joining z_i with z_{i+1} (where indices are taken modulo n). We define the *shape parameter* ζ_i of γ_i to be the cross-ratio

$$\zeta_i = \frac{(z_{i-1} - z_i)(z_{i+1} - z_{i+2})}{(z_{i-1} - z_{i+1})(z_i - z_{i+2})},$$

with the usual rules about cancelling $\pm\infty$ terms. If we perform an isometry of $\mathbb{H}^3$ to place the vertices z_{i-1}, z_i, z_{i+1} at $1, \infty, 0$ respectively, then the vertex z_{i+2} will be placed at ζ_i, and we see that the collection of n shape parameters determines the isometry class of the ideal n–gon.

It follows that for a 3–sided polygon each shape parameter is equal to 1; it is also easy to check that for a 4–sided polygon the sum of two consecutive shape parameters is 1, whence opposite shape parameters are equal. For general n, we may obtain convenient equations relating the ζ_i from the fact that the polygon closes up. Specifically, if we place the polygon so that $z_{i-1} = 1, z_i = \infty, z_{i+1} = 0$, then the isometry ψ_i given by the Möbius transformation $z \mapsto -\zeta_i/(z-1)$ maps z_{i-1}, z_i, z_{i+1} to z_i, z_{i+1}, z_{i+2}, respectively. Since the polygon $\widetilde{\Pi_R}$ closes up, the composite $\psi_n \circ \cdots \circ \psi_2 \circ \psi_1$ must equal the identity, and passing to matrices, we see that we have an identity

$$\begin{bmatrix} 0 & -\zeta_n \\ 1 & -1 \end{bmatrix} \cdots \begin{bmatrix} 0 & -\zeta_2 \\ 1 & -1 \end{bmatrix} \begin{bmatrix} 0 & -\zeta_1 \\ 1 & -1 \end{bmatrix} \sim \begin{bmatrix} 1 & 0 \\ 0 & 1 \end{bmatrix}, \tag{1}$$

where $\sim$ denotes equality up to multiplication by a non-zero scalar matrix. From the $(2,1)$–entry of this product we can read off a polynomial relation $f_n = 0$ in the ζ_i. It is then easily checked, using induction on n, that the polynomials f_n may be defined recursively by

$$f_3 \equiv 1-\zeta_2, \quad f_4 \equiv 1-\zeta_2-\zeta_3, \quad f_n \equiv f_{n-1} - \zeta_n f_{n-2} \quad (n \geq 5). \tag{2}$$

We observe that the polynomial f_n involves the $n-2$ shape parameters $\zeta_2, \zeta_3, \ldots, \zeta_{n-1}$, and that f_n is of degree 1 in each of these shape parameters. In particular, the relation $f_n = 0$ allows one to express each of these $n-2$ shape parameters as a function of the other $n-3$. Let f_n^+ (f_n^-) be the polynomial obtained from f_n by increasing all indices by 1 (resp. decreasing all indices by 1). Then f_n^+ is independent from f_n, as it is the only one of the two that involves ζ_n; also, f_n^- is independent from both f_n and f_n^+, as it is the only one of the three that involves ζ_1. In fact $\{f_n^- = 0, f_n = 0, f_n^+ = 0\}$ must be a complete set of relations for the n shape parameters of a generic ideal n–gon, as the triple transitivity of the action of the group of Möbius transformations on the boundary $\mathbb{C} \cup \{\infty\}$ dictates that the isometry class of an ideal polygon with n sides has $n-3$ geometric degrees of freedom.

It is immediate from the definition of a shape parameter that an ideal polygon lies in a hyperbolic plane if and only if all its shape parameters are real. For highly symmetric links, ideal polygons are often encountered that are *regular*, in the sense that all ζ_i are equal.

Note 2.2 In order to conform to various sign conventions, later we shall be obliged to deal with the *complex conjugates* of shape parameters. However, since complex conjugation is a field automorphism of the complex numbers, these complex conjugates $\overline{\zeta_i}$ satisfy the same polynomial relations as the ζ_i.

Proposition 2.3 *The common shape parameter for a regular n–sided ideal polygon is $\frac{1}{4}\sec^2\frac{\pi}{n}$.*

Proof We may assume that the n ideal vertices of the polygon are evenly spaced around a unit circle in $\mathbb{C}$; specifically, we assume that the ideal vertices are w^i $(0 \leq i \leq n-1)$, where $w = e^{2\pi i/n}$. The cross-ratio of the first four of these points is then

$$\frac{(1-w)(w^2-w^3)}{(1-w^2)(w-w^3)} = \frac{w^2(1-w)^2}{w(1-w^2)^2} = \frac{w}{(1+w)^2}\,.$$

Noting that the line segment joining 0 with $1+w$ is a diagonal of the rhombus with vertices $0, 1, 1+w, w$, we see that the modulus of $1+w$ is $2\cos\pi/n$. Also, since this diagonal bisects the angle of the rhombus at 0, the argument of the above cross-ratio is 0; the result follows. □

It follows from Proposition 2.3 that for regular polygons ζ decreases monotonically to the limit $\frac{1}{4}$ as $n \to \infty$.

In the absence of symmetry, polygons with four or more sides need not be regular, and need not lie in a hyperbolic plane, although for alternating links it seems from experiment that they are close to being planar, and never deviate very far from being regular. Here are two examples of this phenomenon.

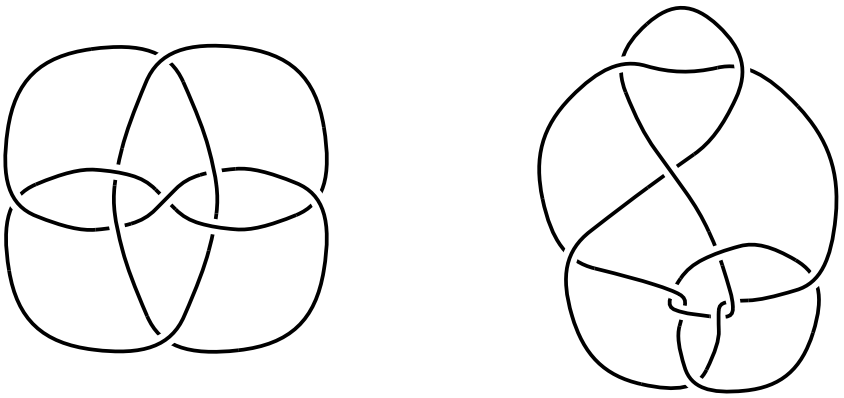

$9a37$ $11a79$

Figure 1

Example 2.4 The knot $9a37$ in the Dowker–Thistlethwaite listing.

There is a symmetry of order 3 cyclically permuting the three regions with four sides. For each of these regions, the shape parameters corresponding to the "north" and "south" crossings are both $0.469789 - 0.090643i$, and the shape parameters corresponding to the "east" and "west" crossings are both $0.530211 + 0.090643i$, these values being rounded to six decimal places. The imaginary parts are seen to be quite small, and the shape parameters are fairly close to that of a regular 4–sided region, namely $\frac{1}{2}$.

Example 2.5 The knot $11a79$ in the Dowker–Thistlethwaite listing.

For the small 5–sided region in the lower-middle part of the diagram, we begin at the top crossing and proceed around the region in a counterclockwise direction. To six decimal places, the five shape parameters for this region are as follows: $0.312331 - 0.008243i$, $0.449632 - 0.007097i$, $0.346369 + 0.018155i$, $0.370339 - 0.024868i$,

$0.432793 + 0.022291i$. This time we compare with the shape parameter of a regular 5–sided ideal polygon, $\frac{1}{4}\sec^2\frac{\pi}{5} = (3-\sqrt{5})/2 \approx 0.381966$.

In the next section we shall see how to use the peripheral structure of the link complement to set up a system of equations for determining the shape parameters of the ideal polygons and for determining how the polygons are situated relative to one another. The unknowns of these equations will be complex numbers attached to the edges and crossings of the diagram; these complex number "labels" will in fact determine the complete hyperbolic structure of the link complement.

3 Edge and crossing labels

We assume throughout that horospherical cross-sections of the cusps have been chosen so that a (geodesic) meridian curve on the cross-sectional torus has length 1. This guarantees (Adams [2]) that cross-sectional tori from distinct cusps are disjoint, and that each torus is embedded in the link complement, with the exception of the figure-eight knot complement, where the cross-sectional torus touches itself in two points.

The preimage of each cross-sectional torus in the universal cover $\mathbb{H}^3$ is a union of horospheres, and we specify a complex affine structure on each horosphere by declaring (for convenience) that meridional translation is through unit distance in the positive real direction. We also would like the translation corresponding to a longitude on the torus to have positive imaginary part, so in order to keep the standard orientation of the complex plane and the usual "right-hand screw" convention relating the directions of meridian and longitude, we view the torus *from the thick part* of the manifold, ie, from the opposite side to the cusp.

We assume that coordinates are chosen so that one of the horospheres is the Euclidean plane H_∞ of (Euclidean) height 1 above the xy–plane, and that it has the standard affine structure; thus on that horosphere the meridional translation is represented by the matrix $\left[\begin{smallmatrix}1 & 1\\ 0 & 1\end{smallmatrix}\right]$.

Now consider an ideal polygon $\widetilde{\Pi_R}$ in $\mathbb{H}^3$, associated to a region R of the link diagram, and with ideal vertices $z_1, \dots, z_n$ as above. Each vertex z_i is the center of a horosphere H_i, and each geodesic edge γ_i of $\widetilde{\Pi_R}$ meets H_i, H_{i+1} in points P_i, Q_{i+1} respectively (Figure 2). At this stage, for book-keeping purposes we need to choose an orientation of the link, and this orientation will determine a direction on the geodesic arc on H_i joining Q_i with P_i. From the affine structure on H_i we now have a complex number determining a translation mapping one of P_i, Q_i to the other, depending on this direction. This complex number is affixed to the side of the

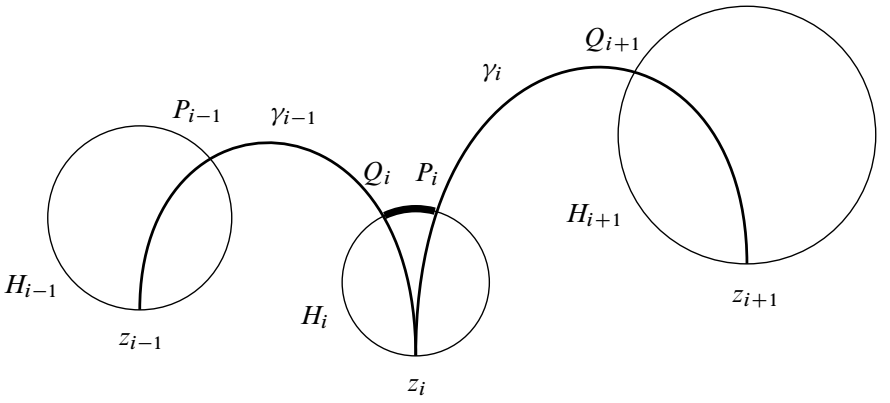

Figure 2

corresponding edge E of the link diagram incident to the region R, and will be called an *edge label*.

Next we note that there is a simple relation between the edge labels on the two sides of an edge E of the link diagram. Let the regions incident to E be R, S, and let the corresponding labels affixed to the two sides of E be u_R^E, u_S^E respectively. These labels correspond to geodesic arcs on a horosphere that descend to arcs α_R^E, α_S^E on the peripheral torus, joining the points of intersection of the torus with two successive crossing geodesics. Let μ denote a meridian curve on the torus, oriented as usual according to the "right-hand screw" rule, and for an arc α let $\overline{\alpha}$ denote its reverse. The loop $\alpha_R^E * \overline{\alpha_S^E}$ is homotopic to $\kappa\mu$, where

$$\kappa = \begin{cases} 1 & \text{if } E \text{ ascends from left to right,} \\ -1 & \text{if } E \text{ descends from left to right,} \\ 0 & \text{if } E \text{ is level,} \end{cases}$$

as one looks from the interior of the region R. It follows that $u_R^E - u_S^E = \kappa$, where κ is as above (see Figure 3, which illustrates the case $\kappa = 1$).

In the case of reduced alternating diagrams, the relation between u_R^E and u_S^E is particularly simple. If we colour the regions in checkerboard fashion, then the view from inside regions of one colour has all edges on the boundary of the region ascending from left to right, and the view from regions of the other colour has edges descending from left to right. We may take the convention that regions of the former type are black, and those of the latter type white. Then, if R is a black region and S is an adjacent white region, we have $u_R^E - u_S^E = 1$.

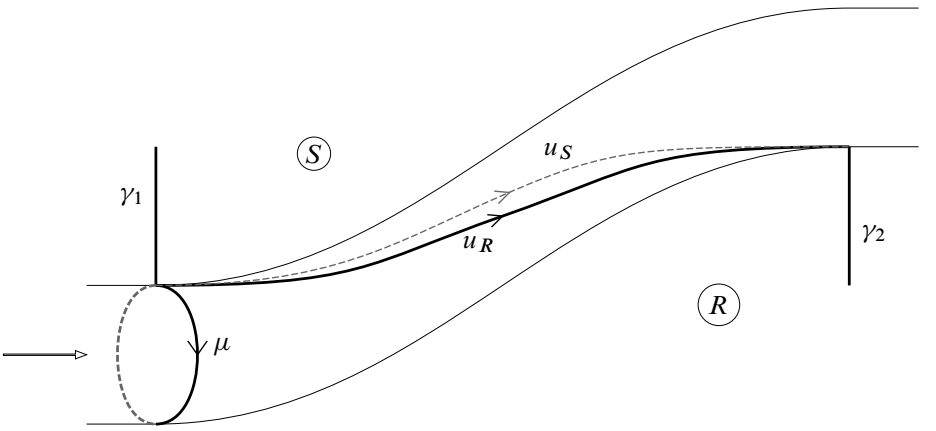

Figure 3

We turn now to crossing labels. To each crossing geodesic γ we assign a complex number w_γ as follows. We lift γ to a geodesic $\widetilde{\gamma}$ in $\mathbb{H}^3$ joining the centers of horospheres H_1, H_2. The meridional direction on H_i $(i = 1, 2)$ together with the geodesic $\widetilde{\gamma}$ defines a hyperbolic half-plane Σ_i containing $\widetilde{\gamma}$, and we define the argument of w_γ by $\arg w_\gamma = \phi_\gamma + \pi$, where ϕ_γ is the angle between the half-planes Σ_1, Σ_2, the sign of ϕ_γ being determined by the convention that a right-handed screw is positive. Thus we have $\arg(-w_\gamma) = \phi_\gamma$; the reason for choosing $-w_\gamma$ here rather than w_γ is explained in the next paragraph. In essence we are defining the angle ϕ_γ as the angle between the two meridional directions by parallel transport along the geodesic $\widetilde{\gamma}$. The specification of w_γ is completed by defining its modulus to be e^{-d}, where d is the hyperbolic length of the part of $\widetilde{\gamma}$ between H_1 and H_2.

If we take H_1 to be the horosphere H_∞ defined above, then $|w_\gamma|$ is the Euclidean diameter of the horosphere H_2. The argument of w_γ may loosely be interpreted as the angle (in the hyperbolic structure) between the overpass and underpass at the crossing in question. The reason for choosing $\phi_\gamma + \pi$ rather than ϕ_γ as the argument of w_γ is illustrated in Figure 4. In that figure are illustrated an overpass and underpass that are parallel; thus, if $\arg(w_\gamma)$ is to measure the angle between these strands, we would like $\arg(w_\gamma)$ to be zero. However, at the top end of the intercusp segment of the geodesic, the direction of the meridian is away from the viewer, whereas at the bottom end the direction of the meridian is towards the viewer.

We note that the isometry represented by the matrix $\left[\begin{smallmatrix} 0 & -w_\gamma \\ 1 & 0 \end{smallmatrix}\right]$ maps H_1 to H_2, respecting affine structures.

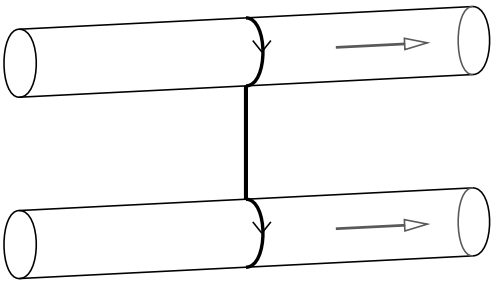

Figure 4

In the degenerate case of a two-sided region, the two arcs travelling from overpass to underpass of the two crossings are parallel, hence are homotopic to the same geodesic. Therefore the two crossing labels are equal, the ideal polygon for this region collapses, and the two edge labels for the region are 0. For taut diagrams, in particular reduced alternating diagrams, we have the following converse:

Theorem 3.1 *Let R be a region of at least three sides of a taut diagram D of a hyperbolic link L. Then each edge label for R is non-zero.*

Proof Suppose that E is some edge of the region R for which the label u_R^E is zero. Let z be the ideal vertex of $\widetilde{\Pi}_R$ corresponding to this edge, and let H be the horosphere centred at z. Since $u_R^E = 0$, the two geodesic edges of $\widetilde{\Pi}_R$ issuing from z meet H in the same point, hence are equal, contradicting Proposition 2.1. □

Conjecture 3.2 Let D be a reduced alternating diagram of a hyperbolic link. Each edge label for D has non-negative imaginary part.

The above definition of crossing labels applies to any geodesic γ travelling from cusp to cusp. Indeed, such a geodesic may be regarded as belonging to a crossing of some diagram of the link.

We conclude this section with a remark on symmetries. Let $h\colon (S^3, L) \to (S^3, L)$ be a homeomorphism; then, modifying h by a homotopy if necessary, we may assume that the restriction of h to $S^3 - L$ is an isometry. Let us suppose that h maps a crossing geodesic γ to γ'. Then the moduli of $w_\gamma, w_{\gamma'}$ will be equal. If h preserves the orientation of S^3, the associated labels $w_\gamma, w_{\gamma'}$ will also have equal arguments, whence $w_{\gamma'} = w_\gamma$; on the other hand, if h reverses the orientation of $S^3 - L$ the argument of w_γ will be negated, whence $w_{\gamma'} = \overline{w_\gamma}$. Edge labels are affected similarly

under the action of h: if h maps a diagram of L to itself and u, u' are edge labels that correspond under the homeomorphism, then $u' = u$ or $u' = \overline{u}$ depending on whether h preserves or reverses the orientation of S^3.

4 The hyperbolicity equations in the edge and crossing labels

We begin with a useful identity. Let R be a region of a link diagram with at least three sides; from Theorem 3.1 this condition ensures that all edge labels for R are non-zero. Let γ be a geodesic edge of the ideal polygon bounding R, let w be the crossing label attached to γ, and let $u_R^{E_1}, u_R^{E_2}$ be the labels for the edges incident to this crossing, the suffix R indicating of course that the labels are placed on the sides of these edges in the region R. Then we have the following relation between the shape parameter ζ_γ and the edge labels $u_R^{E_1}, u_R^{E_2}$:

Proposition 4.1

$$\overline{\zeta_\gamma} = \frac{\kappa w}{u_R^{E_1} u_R^{E_2}}, \tag{3}$$

where $\kappa = 1$ if one edge is directed towards the crossing and one away from the crossing, and where $\kappa = -1$ if both edges are directed towards the crossing or both away from the crossing.

Remark The presence of complex conjugation in $\overline{\zeta_\gamma}$ is merely an artefact of our various sign conventions; as observed in Note 2.2, it is not an obstacle, as the $\overline{\zeta_i}$ satisfy the same relations as the ζ_i. By means of formula (3), each equation in (complex conjugates of) shape parameters may now be regarded as an equation in edge and crossing labels; moreover, by clearing denominators, we may regard these equations as polynomial equations in the labels.

Lemma 4.2 *Figure 5 illustrates a configuration in the hyperbolic plane containing a horocycle of Euclidean diameter D, and geodesics γ_1, γ_2 originating from the centre of the horocycle and meeting the horocycle at points P, Q respectively. The ends of γ_2 are Euclidean distance d apart. Then the hyperbolic distance along the horocycle from P to Q is D/d.*

Proof To obtain the hyperbolic distance along the horocycle from P to Q we perform the isometry that is inversion in the circle C illustrated, with Euclidean centre at the foot of γ_1 and with radius d. This inversion maps γ_1 into itself, maps γ_2 to the geodesic γ_2' illustrated, and maps the horocycle to the Euclidean horizontal line at height d^2/D

above the boundary. The points P, Q are mapped to points P', Q' respectively on this image horocycle, and the circular arc on the horocycle joining P, Q is mapped to the (horizontal) Euclidean line segment joining P', Q'. This line segment has hyperbolic length $d/(d^2/D) = D/d$. □

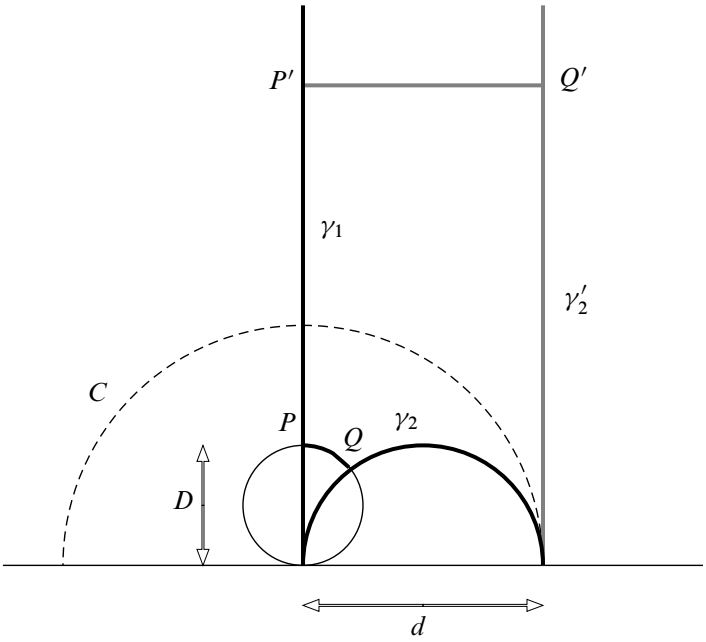

Figure 5

Proof of Proposition 4.1 We shall verify (3) in the case where both edges are directed away from the crossing, in which case $\kappa = -1$. The other cases are then verified simply by changing the sign of one or both of the edge labels.

Let z_0, z_1, z_2, z_3 be consecutive ideal vertices of the ideal polygon corresponding to the region R, such that the geodesic γ joins z_1 to z_2. Applying a suitable isometry of hyperbolic space, we may assume that $z_0 = |u_R^{E_1}|, z_1 = \infty, z_2 = 0$. The horosphere of which z_1 is centre is the Euclidean plane at height 1 above the boundary plane, and the horosphere of which z_2 is centre has diameter $|w|$. Cancelling infinite terms in the usual way, the cross-ratio defining ζ_γ is seen to be z_3/z_0. The situation is illustrated in Figure 6, where μ_1, μ_2 denote meridian vectors, and (for notational simplicity) u_1, u_2 denote $u_R^{E_1}, u_R^{E_2}$ respectively.

First we check that the moduli of the two sides of (3) agree. This follows from Lemma 4.2, applied to the hyperbolic plane containing z_1, z_2, z_3, and where the

quantities of the lemma apply as follows: $\gamma_1 = \gamma$, $D = |w|$, $d = |z_3| = |\zeta_\gamma||u_R^{E_1}|$, and the distance from P to Q along the horocycle is $|u_R^{E_2}|$.

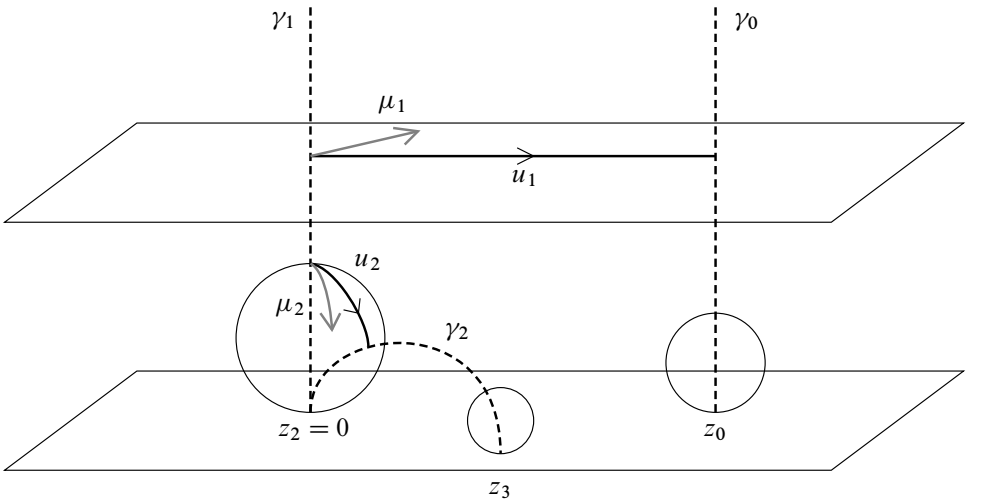

Figure 6

It remains to check that the arguments of the complex numbers on each side of equation (3) match. Figure 6 illustrates the situation where the angle ϕ_{γ_1} between meridian vectors μ_1, μ_2 is approximately $+\pi/2$ and the arguments of u_1, u_2 are each positive acute angles. The ideal vertices z_0, z_1, z_2 are situated at $|u_1|, \infty, 0$ respectively, so $\arg(\zeta_{\gamma_1}) = \arg(z_3)$. Noting that the Euclidean ray from z_2 towards z_0 is in the positive real direction, and taking account of the angles between the four vertical planes through γ_1 containing the vectors μ_1, μ_2, u_1, u_2, we see that

$$\arg(z_3) = \arg(u_1) + \arg(u_2) - \phi_{\gamma_1} = \arg(u_1) + \arg(u_2) - \arg(-w).$$

Therefore, in the notation of the statement of the proposition, we have

$$\arg(\overline{\zeta_\gamma}) = -\arg(z_3) = \arg(-w) - \big(\arg(u_R^{E_1}) + \arg(u_R^{E_2})\big),$$

and the proof is complete. □

The next proposition gives an alternative version of the equation

$$\prod_{i=n}^{1} \begin{bmatrix} 0 & -\zeta_i \\ 1 & -1 \end{bmatrix} \sim I$$

in Möbius transformations for a region with $n \geq 3$ sides, given by Equation (1) of Section 2. This will be useful for the discussion regarding holonomy representations in Section 5.

Proposition 4.3 *Let R be a region of a link diagram with $n \geq 3$ sides, and, starting from some crossing of R, let $u_1, w_1, u_2, w_2, \ldots, u_n, w_n$ be the alternating sequence of edge and crossing labels for R encountered as one travels around the region. Also, for $1 \leq i \leq n$ let $\epsilon_i = 1$ (resp. $\epsilon_i = -1$) if the direction of the edge corresponding to u_i is with (resp. against) the direction of travel. Then the equation in Möbius transformations for R may be written as*

$$\prod_{i=n}^{1} \left(\begin{bmatrix} 0 & -w_i \\ 1 & 0 \end{bmatrix} \begin{bmatrix} 1 & \epsilon_i u_i \\ 0 & 1 \end{bmatrix} \right) \sim \begin{bmatrix} 1 & 0 \\ 0 & 1 \end{bmatrix}. \tag{4}$$

Proof The conclusion follows from (1) in Section 2, together with

$$\begin{bmatrix} 0 & -w_i \\ 1 & 0 \end{bmatrix} \begin{bmatrix} 1 & \epsilon_i u_i \\ 0 & 1 \end{bmatrix} = \begin{bmatrix} 0 & -w_i \\ 1 & \epsilon_i u_i \end{bmatrix} = (-\epsilon_i u_i) T_{i+1}\, M_i\, T_i^{-1},$$

where

$$T_i = \begin{bmatrix} -\epsilon_i u_i & 0 \\ 0 & 1 \end{bmatrix} \quad \text{and} \quad M_i = \begin{bmatrix} 0 & -\frac{w_i}{(\epsilon_i u_i)(\epsilon_{i+1} u_{i+1})} \\ 1 & -1 \end{bmatrix} = \begin{bmatrix} 0 & -\overline{\zeta_i} \\ 1 & -1 \end{bmatrix}. \qquad \square$$

Suppose now that we have a reduced alternating diagram with c crossings. Attached to the diagram are $4c$ edge labels (two for each edge), and c crossing labels, making altogether $5c$ unknowns for our system of equations. The diagram has $c+2$ regions, giving rise to $3(c+2)$ "region" equations in the labels. Together with the $2c$ "edge" equations relating labels on the two sides of an edge, we have in total $5c+6$ equations in $5c$ unknowns. In the next section we examine the relationship between solutions to the equations and representations of the link group into $\mathrm{PSL}_2(\mathbb{C})$.

5 The holonomy representation associated to a solution of the label equations

The connection between solutions to the label equations and parabolic representations of the fundamental group of the link complement into $\mathrm{PSL}_2(\mathbb{C})$ is not quite immediate, but can be established without undue difficulty from first principles, using the classical Wirtinger presentation.

In the traditional picture of the Wirtinger presentation of an oriented link, one takes a diagram of the link that resides in the projection plane apart from vertical perturbations within small neighbourhoods of crossings, and one chooses as basepoint of the link complement some point above the diagram. The generators of the fundamental group of the link complement are then path homotopy classes of loops of form $\alpha_i * \mu_i * \overline{\alpha_i}$, where the path α_i travels in a straight line from the basepoint down to a point a small distance above the i^{th} overpass of the link, μ_i is a small circular loop bounding a disk punctured by the overpass (its direction being determined by the right-hand screw convention), and $\overline{\alpha_i}$ is the reverse of α_i.

For the current context, we shall take the tree that is the union of the α_i, and push it, keeping the terminal ends of the α_i fixed, so that the basepoint lies on the peripheral torus, directly above the i^{th} overpass, and so that each path α_i is a succession of subpaths, each of which either travels along the peripheral torus between crossings or travels along the intercusp segments of crossing geodesics. At this stage the endpoints of the α_i, including the basepoint, are all at the tops of meridional circles on the peripheral torus. It is convenient for purposes of visualization, however, to make a final adjustment to the tree, whereby we drag the endpoints of the α_i halfway around their respective meridional circles so that each lies *underneath* its overpass, on the vertical arc that joins overpass to underpass.

One can imagine a large playground construction consisting of knotted tubes of cross-sectional diameter say 1 metre, and ladders joining underpasses with overpasses; the task of α_i is to travel from one overpass to another by clambering along sections of tube and climbing or descending ladders, in such a way that the union of the α_i is the result of a deformation of the "classical" tree as described above. We note that if we take the first overpass to be that where the basepoint is situated, then we may take α_1 to be the trivial path at the basepoint. Also, we may assume that each subpath of α_i that lies on the peripheral torus is either of the type α_R^E of Section 3 (in which case it corresponds to an edge label), or else is a meridional circle. The reason why meridional circles might be needed is that one is not permitted to travel along an underpass under an overpass, so in order to get past the overpass one would need to climb up to it, travel around a meridional circle and then climb back down before proceeding. Naturally, each subpath that travels along a vertical arc between overpass and underpass corresponds to a crossing label.

The process of deforming the tree $\bigcup \alpha_i$ is illustrated in Figure 7. After the deformation, α_1 has been shrunk to a point, α_2 descends to the underpass at the left-hand crossing before travelling along the peripheral torus to its target overpass, and α_3 travels along the peripheral torus from the basepoint x_0 before ascending vertically to its target overpass.

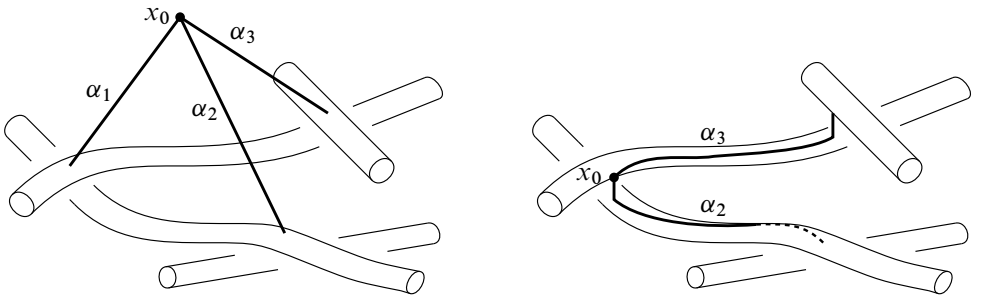

Figure 7

We are now ready to specify the representation $\phi\colon \pi_1(S^3 - L) \to \mathrm{PSL}_2(\mathbb{C})$ associated to a set of labels satisfying the label equations. Each Wirtinger generator $[\alpha_i * \mu_i * \overline{\alpha_i}]$ will map to a conjugate of the parabolic $\left[\begin{smallmatrix} 1 & 1 \\ 0 & 1 \end{smallmatrix}\right]$ by a matrix M_i determined by the path α_i. Evidently there are choices involved in how the "classical" tree is pushed to its present form; one can travel in either of two ways around a region between two crossings incident to that region; however, it will be seen from the definition of M_i given shortly that independence of those choices is guaranteed by the label equations, in the form given in (4) of Proposition 4.3.

Let us write α_i as a concatenation of subpaths $\alpha_i^1 * \alpha_i^2 * \cdots * \alpha_i^{n_i}$, where each subpath is of one of the three types: (i) corresponds to an edge label, (ii) is a meridional circle, (iii) corresponds to a crossing label. The standard process of lifting the loop $\alpha_i * \mu_i * \overline{\alpha_i}$ to $\mathbb{H}^3$ dictates that we define $M_i = M_i^1 M_i^2 \cdots M_i^{n_i}$, where

$$M_i^{\,j} = \begin{cases} \begin{bmatrix} 1 & \pm u \\ 0 & 1 \end{bmatrix} & (\alpha_i^j \text{ corresponds to the edge label } u, \text{ the sign being } +1 \text{ if and only if the direction of the edge agrees with that of } \alpha_i), \\ \begin{bmatrix} 1 & \pm 1 \\ 0 & 1 \end{bmatrix} & (\alpha_i^j \text{ is a meridional circle, the sign determined by the RH screw rule}), \\ \begin{bmatrix} 0 & -w \\ 1 & 0 \end{bmatrix} & (\alpha_i^j \text{ corresponds to the crossing label } w). \end{cases}$$

Finally, the image of the i^{th} Wirtinger generator is given by

$$\phi([\alpha_i * \mu_i * \overline{\alpha_i}]) = M_i \begin{bmatrix} 1 & 1 \\ 0 & 1 \end{bmatrix} (M_i)^{-1}.$$

There now follows an illustration of the construction of the representation ϕ. The solutions of the label equations for the Turk's head knot (Figure 8) are obtained in

Example 6.2 below, in the case $n = 4$. As explained in that example, there are two geometric solutions (forming a complex conjugate pair) and two real non-geometric solutions.

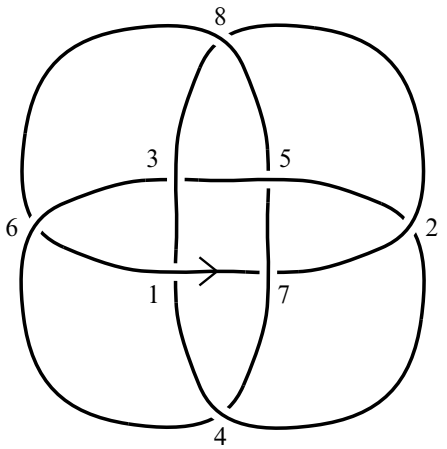

Figure 8

In Figure 8, the overpasses are labelled from 1 to 8, in order around the knot. From the knot's symmetry, the four edge labels for the central 4–sided region are equal, as are that region's four crossing labels. Let us denote the common edge label for this region u, and the common crossing label w. A quick study of the Wirtinger presentation for this diagram reveals that the knot group is generated by the Wirtinger generators at overpasses labelled $1, 7, 5$; let us denote these generators a, b, c respectively, and let us use upper-case A, B, C to denote their inverses. The defining relators for the group (also obtained from the Wirtinger presentation) are then

$$r_1 = BabACbcBabCBcaBAbC,$$
$$r_2 = ACbcBabCBcaCbcBAbCBcbcBabCBcACbcBAbCBcaB;$$

we could of course have had much shorter relators at the expense of a larger generating set.

If we put the basepoint at overpass 1, then we can get to overpass 7 by travelling along the part of the peripheral torus corresponding to the lower edge of the central 4–sided region, followed by a climb from the underpass to the overpass at the crossing labelled 7. In order to get to overpass 5, we have to repeat this process, travelling along the right-hand edge of the central 4–sided region. The conjugating matrices for the

generators b, c are therefore

$$M_b = \begin{bmatrix} 1 & u \\ 0 & 1 \end{bmatrix} \begin{bmatrix} 0 & -w \\ 1 & 0 \end{bmatrix}, \quad M_c = M_b^2.$$

From the computation in Example 6.2, the values of u for each of the four solutions are:

$$\frac{-1+i\sqrt{4\sqrt{2}-5}}{\sqrt{2}}, \quad \frac{-1-i\sqrt{4\sqrt{2}-5}}{\sqrt{2}}, \quad \frac{1+\sqrt{4\sqrt{2}+5}}{\sqrt{2}}, \quad \frac{1-\sqrt{4\sqrt{2}+5}}{\sqrt{2}},$$

these being the roots of the polynomial $x^4 - 6x^2 - 8x - 4$. It is evident from the regularity of the central 4–sided region that in each case $w = \frac{1}{2}u^2$. Also, from our choice of basepoint, in each case $\phi(a) = \left[\begin{smallmatrix} 1 & 1 \\ 0 & 1 \end{smallmatrix}\right]$. For the first solution, we find that

$$\phi(b) = \begin{bmatrix} \frac{1}{\sqrt{2}}\left(2\sqrt{2}+1+i\sqrt{2\sqrt{2}+1}\right) & 2 \\ \frac{1}{2}\left(-1-i\sqrt{11+8\sqrt{2}}\right) & \frac{1}{\sqrt{2}}\left(-1-i\sqrt{2\sqrt{2}+1}\right) \end{bmatrix},$$

$$\phi(c) = \begin{bmatrix} \frac{1}{\sqrt{2}}\left(2\sqrt{2}+1+i\sqrt{2\sqrt{2}+1}\right) & 1 \\ -1-i\sqrt{11+8\sqrt{2}} & \frac{1}{\sqrt{2}}\left(-1-i\sqrt{2\sqrt{2}+1}\right) \end{bmatrix},$$

and for the (non-geometric) third solution

$$\phi(b) = \begin{bmatrix} \frac{1}{\sqrt{2}}\left(2\sqrt{2}-1-\sqrt{2\sqrt{2}-1}\right) & 2 \\ \frac{1}{2}\left(-1+\sqrt{-11+8\sqrt{2}}\right) & \frac{1}{\sqrt{2}}\left(1+\sqrt{2\sqrt{2}-1}\right) \end{bmatrix},$$

$$\phi(c) = \begin{bmatrix} \frac{1}{\sqrt{2}}\left(2\sqrt{2}-1-\sqrt{2\sqrt{2}-1}\right) & 1 \\ -1+\sqrt{-11+8\sqrt{2}} & \frac{1}{\sqrt{2}}\left(1+\sqrt{2\sqrt{2}-1}\right) \end{bmatrix}.$$

Representations corresponding to the other two solutions may be constructed similarly. That all four representations satisfy the relations $r_1 = 1, r_2 = 1$ may be verified using software such as Maple or Mathematica.

Clearly the induced parabolic representation of the link group into $\mathrm{PSL}_2(\mathbb{C})$ is a continuous function of the edge and crossing labels; also, a variation of the labels within the solution space would change the geometry of the link complement. Therefore from Mostow–Prasad rigidity we have:

Theorem 5.1 *The solution of the label equations corresponding to the geometric structure is isolated.*

Conjecture 5.2 For hyperbolic alternating links, the solution space of the label equations is 0–dimensional, whence the same is true of the space of parabolic representations of the link group into $\mathrm{PSL}_2(\mathbb{C})$.

Since the label equations have a reasonably pleasant form for alternating diagrams, it is reasonable to hope that a proof of Theorem 5.1, and indeed of Conjecture 5.2, can be found without recourse to Mostow–Prasad rigidity.

We do not know of a simple test for deciding which solution of the equations corresponds to the geometric structure; however, by subdividing the link complement into ideal tetrahedra and keeping track of labels, one may compute the volume of the representation given by the solution, and the solution with the greatest volume will be the geometric solution (Francaviglia [9]). Empirically, for alternating links the geometric solution is that for which the "region" ideal polygons are closest to being regular.

Experimentally, the near-regularity of these polygons is particularly evident for alternating diagrams of so-called Conway basic polyhedra, these being links possessing alternating diagrams with no two-sided region. The simplest examples are (i) the Borromean rings, (ii) the Turk's head knot, (iii) the 9–crossing knot denoted 9* by J H Conway in [7] (listed as 9_{40} in Rolfsen [16] and as $9a37$ in the Dowker–Thistlethwaite classification).

For the Borromean rings, the regions are forced to be regular by virtue of being 3–sided, and regularity of the 4–sided regions of the Turk's head knot is a consequence of the symmetries of that knot; see Example 6.2 below. On the other hand, as already seen in Example 2.4, the knot 9* (Figure 1) has 4–sided regions that deviate slightly from being regular.

6 Examples

In this section we give some examples illustrating the use of the hyperbolicity equations from Section 4.

6.1 The figure-eight knot

Recall that for a 3–sided region all shape parameters are 1. Regions I, II, III each provide three equations in the labels, as follows:

$$\text{I:}\quad w_2 = -(u_2+1),\ w_2 = -(u_1+1),\ w_1 = (u_1+1)(u_2+1)$$
$$\text{II:}\quad w_1 = u_2,\ w_1 = u_3,\ w_2 = u_2u_3$$
$$\text{III:}\quad w_2 = -(u_3+1),\ w_2 = -(u_4+1),\ w_1 = (u_3+1)(u_4+1)$$

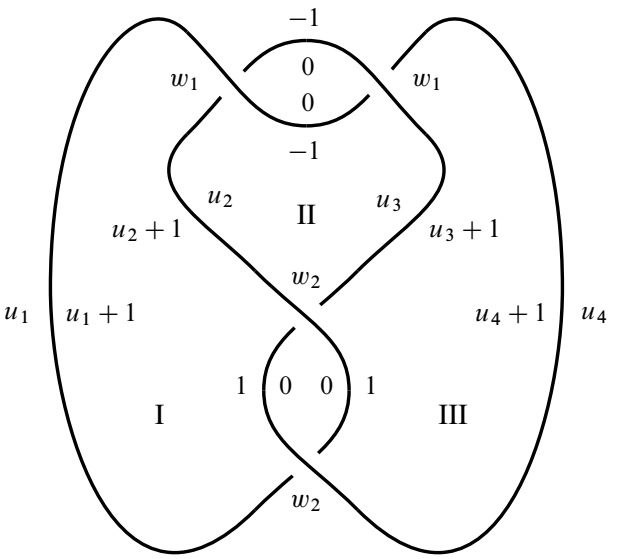

Figure 9

Collecting these results, we obtain

$$w_1 = u_1 = u_2 = u_3 = u_4, \quad u_1^2 + u_1 + 1 = 0, \quad w_2 = -(u_1 + 1), \quad w_1 = w_2^2 .$$

Therefore, without loss of generality, we have

$$u_1 = u_2 = u_3 = u_4 = \tfrac{1}{2}(-1 + i\sqrt{3}), \quad w_1 = \tfrac{1}{2}(-1 + i\sqrt{3}), \quad w_2 = \tfrac{1}{2}(-1 - i\sqrt{3}).$$

6.2 The closure L_n of the braid $(\sigma_1\sigma_2^{-1})^n$, $n \geq 3$

In Figure 10(i) we have exploited symmetries of the link L_n in order to economize on labels. For notational convenience let λ_n denote $\frac{1}{2}\sec\frac{\pi}{n}$, the positive square root of the shape parameter of a regular ideal n–gon. Looking at Figure 10(i), from the right-hand n–sided region we have

$$w = \lambda_n^2 u_1^2 ,$$

and from 3–sided regions we have

$$w = -(u_1 + 1)(u_2 + 1), \quad w = u_2^2 .$$

Thus $u_1 = \pm(1/\lambda_n)u_2$; however, for the geometric solution we must take $u_1 = (1/\lambda_n)u_2$, as otherwise all edge labels will turn out to be real, resulting in a collapse

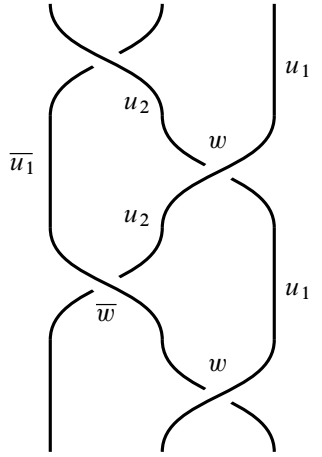

(i) A section of the braid

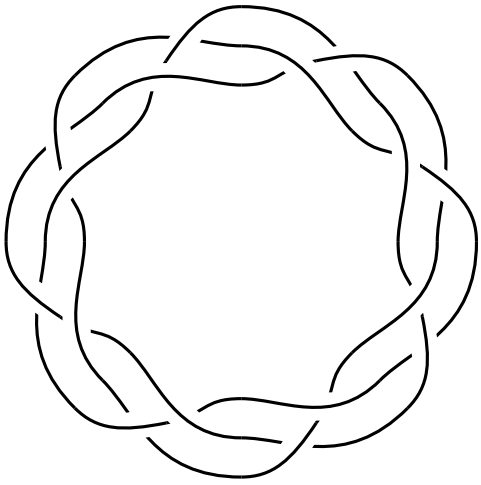

(ii) The closure of $(\sigma_1\sigma_2^{-1})^8$

Figure 10

of the peripheral structure. It then follows quickly that u_2 satisfies

$$\Big(1+2\cos\frac{\pi}{n}\Big)u_2^2+\Big(1+2\cos\frac{\pi}{n}\Big)u_2+1=0,$$

the two solutions of this quadratic yielding geometric structures corresponding to the two orientations of the link complement.

If n is divisible by 3, L_n is a link of 3 components, with symmetries acting transitively on the set of components; otherwise L_n is a knot. The link L_3 is the Borromean rings, and L_4 is the Turk's head knot. In the case of the Borromean rings, the crossing labels are $\pm i/2$, indicating that the overpass and underpass at each crossing are perpendicular to one another; this is also evident from the extra symmetries possessed by this link.

It is of some interest to note that as $n\to\infty$, $|w|\to\frac{1}{3}$. This has the following interpretation in terms of meridian lengths. Let us expand cusp cross-sections, keeping meridian lengths equal, until their union just ceases to be embedded in the link complement (in the case where L_n is a knot the cusp will touch itself). Let ℓ_n denote the length of a meridian on one of these expanded cusp cross-sections; then ℓ_n tends to a limit $\sqrt{3}$ as $n\to\infty$.

Another interesting aspect of the links L_n concerns the canonical cell decompositions (Epstein and Penner [8]) of their complements. The alternating diagram of L_n exhibits a decomposition of the link complement into two congruent ideal polyhedra, one "above" and one "below" (Aitchison, Lumsden and Rubinstein [4]), and this decomposition is

precisely the canonical cell decomposition, as is readily verified by examination of the horoball pattern. See also the discussion of canonical cell decompositions in Sakuma and Weeks [18].

The ideal polygons corresponding to the regions of the alternating diagram of L_n are all regular, hence also planar (compare with the knot 9*, discussed in Example 2.4).

6.3 Three-punctured sphere

Let us consider the three-punctured sphere S in the configuration of Figure 11, with meridional punctures at the two parallel vertical strands, and with a longitudinal puncture at the circular link component. It is well-known (Adams [1]) that we may take S to be a totally geodesic surface, constructed by gluing two ideal triangles together along their edges. If we choose cusps of an ideal triangle so that the length of each cusp boundary is 1, then these cusp boundaries will be tangent to one another; therefore if we choose cusps of a three-punctured sphere so that each cusp boundary is a circle of length $1+1=2$, these circles will touch one another. If we now retract the cusps of the three-punctured sphere so that their boundaries have length 1, the intercusp length of each of the three geodesics joining distinct punctures will be $\log(4)$. Since by convention our meridians always have length 1, it follows that w_3, the label for the geodesic represented by the horizontal line at the top of Figure 11, has modulus equal to $\frac{1}{4}$ (recall from the remark following Conjecture 3.2 that to any geodesic joining cusps there is an associated complex number, defined exactly as crossing labels are defined). On the other hand, since the three-punctured sphere is totally geodesic, the meridians belonging to the vertical strands lie in the same hyperbolic plane as this geodesic, whence $w_3=\frac{1}{4}$. (*Note*: Here we have chosen orientations of the strands so that they are parallel; were they anti-parallel, instead we would have $w_3=-\frac{1}{4}$.)

From the 4–sided region marked I, from the relation f_4 in shape parameters given in Section 2, we have

$$-\frac{w_1}{u_2}-\frac{w_1}{u_1}=1, \quad -\frac{w_1}{u_1}+\frac{w_2}{u_1}=1, \quad \frac{w_2}{u_1}+\frac{w_2}{u_2}=1,$$

from which it follows easily that

$$w_2=-w_1 \quad \text{and} \quad u_1=u_2=-2w_1.$$

Then, from the 3–sided region marked II, we have

$$w_3=\frac{-w_1w_2}{u_1^2}=\frac{1}{4},$$

thus recovering the result obtained by the geometric argument of the previous paragraph.

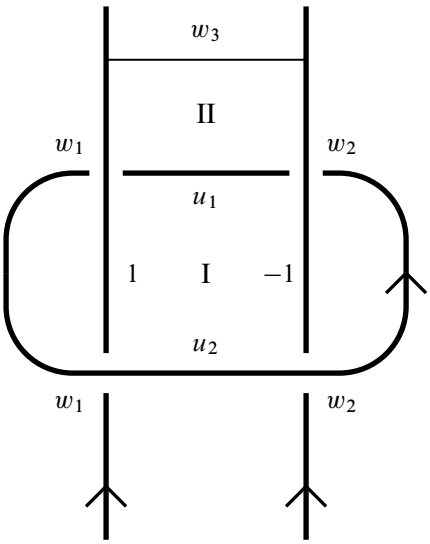

Figure 11

7 Labels on tangles

Let L be a hyperbolic link in S^3. In this section we are concerned with tangles $(B, T) \subset (S^3, L)$, where B is a 3–ball and T is a properly embedded 1–dimensional submanifold of B meeting the boundary of B transversely in four points. Thus $\partial B - \partial T$ is a 4–punctured sphere; we require that this "Conway sphere" be essential in $S^3 - L$. Thus both (B, T) and the complementary tangle $(\overline{S^3 - B}, \overline{L - T})$ are *non-trivial* in the sense of Lickorish [11], ie, neither is homeomomorphic as a pair to (B_0, T_0), where

$$B_0 = \{(x_1, x_2, x_3) \in \mathbb{R}^3 : x_1^2 + x_2^2 + x_3^2 \leq 1\},$$
$$T_0 = \{(x_1, x_2, x_3) \in B_0 : x_2 = 0 \text{ and } x_3 = \pm\tfrac{1}{2}\}.$$

The restriction of the hyperbolic metric on $S^3 - L$ to $B - T$ is complete (in the sense that Cauchy sequences converge), as is the restriction to the 4–punctured sphere $\partial B - \partial T$.

Our first observation is that the boundary of (B, T) enjoys a certain kind of symmetry, which can be described as follows. Let us suppose that B is a standard 3–ball meeting the projection plane in an equatorial disk Δ, and that the tangle T is contained in this disk except for small vertical perturbations at crossings; thus the four boundary points of T are contained in the circle $C = \partial\Delta$. Let these points, taken in cyclic order around

C, be Q_1, Q_2, Q_3, Q_4. If our tangle diagram is part of a taut link diagram, then for each $i \in \{1,2,3,4\}$ we have a complex number $w_{i,i+1}$ associated to the sub-arc of C joining Q_i to Q_{i+1} (suffixes taken modulo 4).

Proposition 7.1 *In the notation of the previous paragraph,* $w_{1,2} = w_{3,4}$ *and* $w_{2,3} = w_{4,1}$.

Proof This follows essentially from the results of D Ruberman in [17]. In that paper it is shown that if we take the Conway sphere $\partial B - \partial T$ to be of least area in its homotopy class, then an involution of mutation is a local isometry near $\partial B - \partial T$. We apply this result to the mutation τ corresponding to a half-turn about an axis perpendicular to the projection plane. In the notation of the previous paragraph, let $\alpha_{i,i+1}$ be the interior of the sub-arc of C joining Q_i to Q_{i+1}; then we may assume that the $\alpha_{i,i+1}$ lie on the least area Conway sphere and that the involution τ interchanges neighbourhoods in $S^3 - L$ of opposite pairs of these arcs. τ also interchanges intersections of these neighbourhoods with our chosen horospherical cusp boundaries.

It is sufficient to check that $w_{1,2} = w_{3,4}$, as the other equality will follow simply by shifting indices. In order to check that $w_{1,2} = w_{3,4}$ holds, we need to compare the relative positions of horospheres at each end of a lift $\widetilde{\alpha_{1,2}}$ of $\alpha_{1,2}$, with those at each end of a lift $\widetilde{\alpha_{3,4}}$ of $\alpha_{3,4}$. Since the involution interchanges open patches of cusp boundaries, it follows that there is an isometry of $\mathbb{H}^3$ mapping the pair of horospheres at the ends of $\widetilde{\alpha_{1,2}}$ to the pair at the ends of $\widetilde{\alpha_{3,4}}$; we conclude that $|w_{1,2}| = |w_{3,4}|$. Equality of the respective arguments of $w_{1,2}, w_{3,4}$ follows from consideration of the action of τ on the affine structures on the open patches of cusp boundaries. Indeed, τ maps meridian curves at Q_1, Q_2 to meridian curves at Q_3, Q_4, and since the tangle has two inward-pointing ends and two outward-pointing ends, τ either preserves or reverses both of their orientations. □

Remark The conclusion of Proposition 7.1 holds also for diagrams of tangles that are trivial in the sense of [11]. This can be established directly from the equations governing edge and crossing labels, by taking the diagram to be of standard 4–plait "rational tangle" form [7] and proceeding by induction on the number of crossings of the 4–plait, the inductive step corresponding to the addition of a crossing by performing a half-twist of two adjacent ends of the tangle. The basis for the induction is the conclusion for a tangle diagram of a single crossing, with crossing label w; there each arc $\alpha_{i,i+1}$ is homotopic to the arc travelling vertically from underpass to overpass at the crossing, whence each $w_{i,i+1}$ is equal to w.

Corollary 7.2 *If a crossing* c_1 *is traded for a crossing* c_2 *by a flype of the link diagram, then the crossings* c_1, c_2 *have equal crossing labels.*

Proof With appropriate numbering, the crossing labels for c_1, c_2 are precisely $w_{1,2}$, $w_{3,4}$ for the tangle turned upside-down by the flype (see Figure 12). □

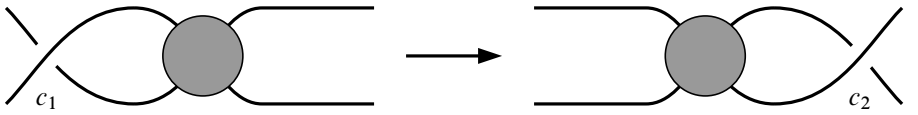

Figure 12: A flype: the tangle represented by the shaded disk is rotated through a half-turn about a horizontal axis, untwisting the left-hand strands and twisting the right-hand strands, thus trading the crossing c_1 for the crossing c_2.

We turn now to consideration of complete hyperbolic structures on a tangle complement $B-T$. Given a solution to the equations in edge and crossing labels corresponding to the regions of a diagram of the tangle, the method of Section 5 will yield a corresponding parabolic representation of the fundamental group of $B-T$ into $\mathrm{PSL}_2(\mathbb{C})$. Here we are considering a tangle pair (B,T) in isolation, not necessarily contained in a link pair (S^3,L).

To avoid dealing with manifolds with non-compact boundary (in this case a 4–punctured sphere), the appropriate setting for investigating the Teichmüller space of complete hyperbolic structures on a tangle complement is that of a *pared manifold* (Morgan [15]; see also Canary and McCullough [6]): one constructs a manifold M, homotopy equivalent to $B-T$ and with compact boundary, by excising from B the interior of a regular neighbourhood of T; the boundary $P\subset\partial M$ of this regular neighbourhood is marked as being peripheral, and is termed the *parabolic locus* of the pared manifold (M,P). The reader is referred to [15, Definition 4.8] for details.

From a discrete faithful parabolic representation of $\pi_1(B-T)$ into $\mathrm{PSL}_2(\mathbb{C})$, or equivalently a discrete faithful representation of $\pi_1(M)$ into $\mathrm{PSL}_2(\mathbb{C})$ mapping elements of $\pi_1(P)$ to parabolics, one obtains a complete hyperbolic structure on the pared manifold (M,P).

Proposition 7.3 *Let (M,P) be a pared manifold arising from a tangle pair (B,T) as above. Then* (i) *the space $\mathcal{T}$ of complete hyperbolic structures on (M,P), if non-empty, is homeomorphic to $\mathbb{R}^2$, and* (ii) *$\mathcal{T}$, regarded as a set of solutions of the label equations for a given taut diagram of (B,T), is an open subset of the space of all solutions of the label equations.*

Proof It follows from a classical result of L Bers [5] (see also [15, Theorem 9.2]) that there is a homeomorphism from the space of complete hyperbolic structures on (M, P) to the Teichmüller space of complete, finite area hyperbolic structures on $\partial M - P$. Since $\partial M - P$ is homeomorphic to a 4–punctured sphere, part (i) follows from the well-known fact that the Teichmüller space of finite area complete hyperbolic metrics on a 2–sphere with n punctures ($n \geq 3$) is homeomorphic to $\mathbb{R}^{2n-6}$. Part (ii) follows directly from the deformation theorem in Marden's [12, Section 6.4]; indeed, Marden's theorem also tells us that $\mathcal{T}$ is a connected, complex analytic manifold of dimension 1, consistent with part (i) of Proposition 7.3. □

The Kleinian group Γ that is the image of $\pi_1(M)$ in $\mathrm{PSL}_2(\mathbb{C})$ can act either on the universal cover $\widetilde{M}$, or on the whole of $\mathbb{H}^3$. In the former case we obtain a hyperbolic metric on M, and the latter provides a complete hyperbolic metric on $\mathbb{H}^3/\Gamma \cong M - \partial M$; these two scenarios can be considered to be in some sense equivalent.

The following two-part remark is tangential to the main discussion, but may be of some interest.

Remark (i) From Proposition 7.1, it follows that if $(B, T) \subset (S^3, L)$ for some hyperbolic link L, and if the boundary 4–punctured sphere of (B, T) is essential in $S^3 - L$, then the numbers $w_{i,j}$ for T arising from the geometric structure on $S^3 - L$ obey the symmetry property $w_{1,2} = w_{3,4}$, $w_{2,3} = w_{4,1}$. Thus this property of the $w_{i,j}$ holds for those points of the Teichmüller space $\mathcal{T}$ that correspond to the situation where we sum (B, T) with a non-trivial tangle to form (S^3, L) for some hyperbolic link L. In fact, if $\mathcal{T} \neq \varnothing$ there are infinitely many such points of $\mathcal{T}$, as one can form infinitely many distinct hyperbolic links L by summing T with an infinite sequence of pairwise distinct non-trivial tangles. From Marden's deformation theorem, $\mathcal{T}$ has complex dimension 1, so $w_{1,2}, w_{3,4}$ cannot be algebraically independent over $\mathcal{T}$. The fact that $w_{1,2} = w_{3,4}$ holds for infinitely many points of $\mathcal{T}$ then implies that the equality holds for all points of $\mathcal{T}$; likewise, $w_{2,3} = w_{4,1}$ throughout $\mathcal{T}$.

(ii) Suppose that we have diagrams of tangles T_1, T_2, with respective solutions S_1, S_2 to the label equations for these diagrams. The numbers $w_{i,j}$ of Proposition 7.1 are then determined for each diagram. Suppose that we form a link diagram by summing together T_1 and T_2; then the solutions S_1, S_2 can be amalgamated to create a solution to the label equations for this link if and only if corresponding $w_{i,j}$ for the two tangles agree. In the case of geometric solutions, we can think of $w_{1,2}, w_{2,3}$ for each T_i as defining a complex curve in $\mathbb{C}^2$; the two curves then meet generically at a point, this point corresponding to the complete structure on the link complement.

We turn our attention to a particular kind of tangle, endowed with a surprising rigidity property.

Definition 7.4 A tangle T conforming to Figure 13(i) will be called an *encircled tangle*, and a diagram of that type will be called a *standard diagram* of an encircled tangle. In that figure, the shaded disk represents an arbitrary tangle U, and T is the union of U and a simple closed curve C that weaves around the ends of U in alternating fashion.

Definition 7.5 Let T be an encircled tangle as above, with encircling simple closed curve C. We assume that T is represented by a standard diagram, ie, one conforming to Figure 13(i). The four crossing labels attached to crossings of C, and four edge labels attached to the *insides* of the edges of C will be called *boundary labels*, and the remaining labels of T interior to C will be called *interior labels.*

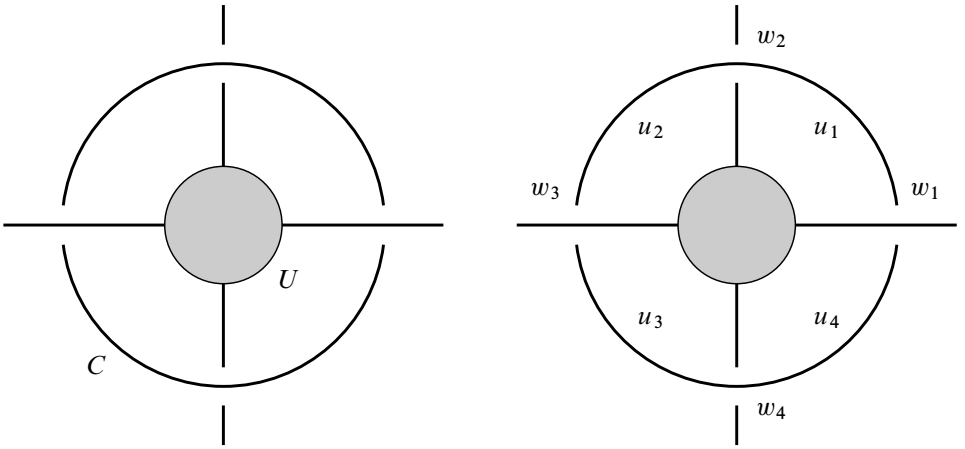

(i) An encircled tangle (ii) Boundary labels

Figure 13

The next theorem expresses the rigidity property for encircled tangles. As before, we denote by $\mathcal{T}$ the space of complete hyperbolic structures on $B-T$. From Proposition 7.3, $\mathcal{T} \cong \mathbb{R}^2$, and we may regard $\mathcal{T}$ as an open subspace of the solution space of the label equations.

Theorem 7.6 (i) *Each interior label of T is constant over $\mathcal{T}$.*

(ii) *Let S_1, S_2 be solutions of the label equations corresponding to points of $\mathcal{T}$. There exists a non-zero complex number k such that if ζ is a boundary label of T in the solution S_1, then the corresponding boundary label in the solution S_2 is $k\zeta$.*

Proof We assume that the diagram of the subtangle U of T (Figure 13) has at least one crossing; thus each region of the tangle diagram incident to the encircling curve C has at least three sides, and shape parameters for these regions are defined. The simple case where U has no crossings will be dealt with directly from the label equations in the proof of Theorem 7.7 below.

Recall that the shape parameter at a corner of a region is, up to sign, the quotient of the label at that crossing by the product of the two incident edge labels. If we take any non-zero complex number k and replace each boundary label of T in S_1 by its product with k, by inspection of Figure 13(ii) all shape parameters for T are unchanged, and the equations given by the regions of the tangle T are still satisfied.

Let $\mathcal{C}$ be the component of the solution set of the label equations that contains $\mathcal{T}$; $\mathcal{C}$ has the structure of a complex algebraic set. From Marden's deformation theorem [12], $\mathcal{T}$ is open in $\mathcal{C}$, consists only of smooth points of $\mathcal{C}$, and has real dimension 2; it follows that $\mathcal{C}$ has complex dimension 1, ie, is a complex algebraic curve, and that $\mathcal{T}$ is away from any singular points of $\mathcal{C}$. Let z_0 be any point of $\mathcal{T}$ (regarded as a subset of $\mathcal{C}$), and let $\mathcal{C}' \subset \mathcal{C}$ be the set of solutions obtained by taking a non-zero complex number k and then multiplying all boundary labels for z_0 by k, but keeping interior labels fixed, as in the previous paragraph (thus k varies over $\mathcal{C}'$). Since $\mathcal{T} \subset \mathcal{C}$ and $\mathcal{C}$ has complex dimension 1, k must parametrize the set $\mathcal{T}$; in particular, $\mathcal{T} \subset \mathcal{C}'$. Both parts of the theorem follow. □

To summarize informally, $\mathcal{T}$ has one complex "degree of freedom", and because of dimensional constraints, this "structural flexibility" has to be parametrized by k. Thus the complete structures of an encircled tangle are related in a simple way; however, we do not know how to determine which values of k, applied in this manner to the particular complete structure z_0, yield points of $\mathcal{T}$.

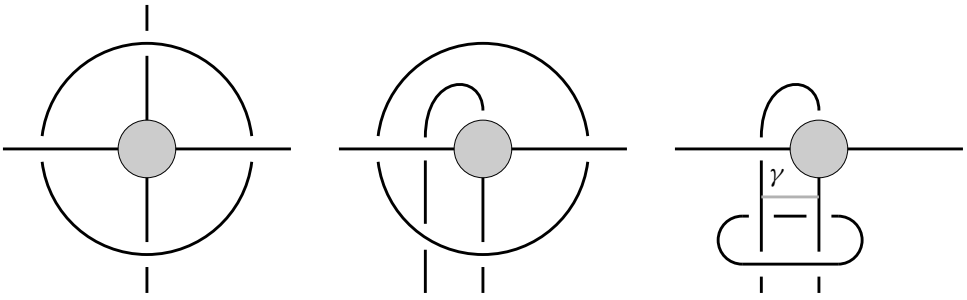

Figure 14

It is perhaps enlightening to give a heuristic, more geometric explanation of this phenomenon. The sequence of diagrams in Figure 14 shows that the encircling simple closed curve bounds a disk Δ meeting L_i in C together with two transverse "punctures". $\Delta - L_i$ is thus a 3–punctured sphere in the link complement, and it follows from Example 6.3 above that the geodesic marked γ in the final diagram of Figure 14 has associated label $\pm\frac{1}{4}$, independent of the link (S^3, L_i) containing (B, T). This imposes an extra constraint (of complex dimension 1) on the geometric structure of the sub-tangle U, making it plausible that its structure is determined uniquely.

The boundary labels of an alternating encircled tangle are subject to further constraints, as expressed in the next theorem. With a little more effort the conclusion can be established without the hypothesis that the tangle be alternating; however, our main interest here is with alternating links.

Theorem 7.7 *Let (B, T) be an alternating encircled tangle, represented by a standard diagram with boundary labels u_i, w_i $(1 \le i \le 4)$, as in Figure 13(ii).*

(i) *The boundary crossing labels w_i are all equal up to sign, any two being equal if and only if the crossings to which they belong have equal sign (see Figure 15).*

(ii) *Opposite boundary edge labels are equal, ie, in Figure 13(ii) $u_1 = u_3$ and $u_2 = u_4$.*

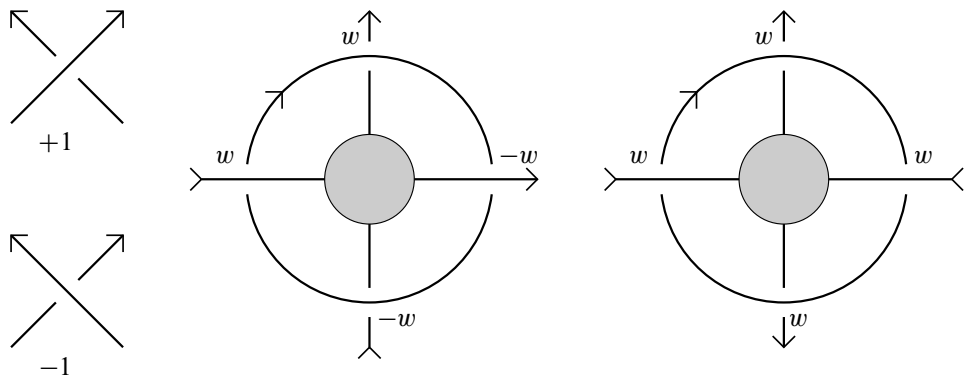

Crossing signs

Figure 15

Proof We first observe that conclusions (i), (ii) hold for the oriented encircled tangles V_1, V_2 illustrated in Figure 16. This may easily be verified from the label equations associated to the 4–sided region interior to the tangle. For example, for V_1 we have $u_1 = u_3 = 0$, $w_1 = w_2$, $w_3 = w_4$, together with the equations

$$\frac{w_3}{u_2} + \frac{w_3}{u_4} = 1\,, \quad -\frac{w_1}{u_2} - \frac{w_1}{u_4} = 1, \quad \frac{w_3}{u_2} - \frac{w_1}{u_2} = 1, \quad \frac{w_3}{u_4} - \frac{w_1}{u_4} = 1;$$

it then follows that $u_2 = w_3 - w_1 = u_4$ and $w_3 = -w_1 = u_2/2$. If we switch the crossings of V_1, the edge labels marked 1 both become -1, but the result of the computation is unaffected. In the case of V_2, it is shown similarly that $u_2 = u_4$ and $w_1 = w_2 = w_3 = w_4 = -u_2/2$.

Now suppose that T is an encircled, oriented tangle distinct from V_1, V_2. Then we may form an alternating hyperbolic link L by summing T with a trivial tangle (Figure 16). We then see that T shares its encircling link component with a copy of one of V_1, V_2. The conclusion for T then follows from the analysis of the V_i in the previous paragraph, together with Theorem 7.6(ii). □

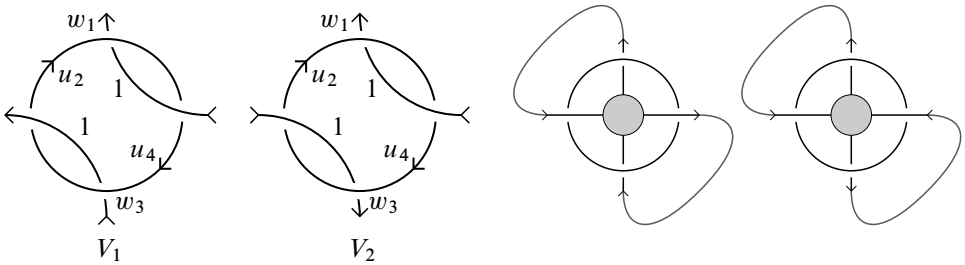

Figure 16

8 Epilogue

It had been observed by the first author that the horoball patterns of alternating links had certain "elements of predictability", and that in many cases one could even reconstruct a diagram for the link by visual inspection of the horoball pattern. The original purpose of the method outlined in this paper was to search for an explanation of this behaviour. For alternating diagrams the hyperbolicity equations relate to the diagram in a natural way, and it is perhaps reasonable to hope that the method will lead eventually to a deeper understanding of the geometry of prime alternating links.

Acknowledgments

The authors are grateful to Colin Adams, Francis Bonahon, David Futer, Darren Long and Jessica Purcell for valuable conversations. Particular thanks are due to the referee, whose extremely helpful and detailed comments have played an essential part in the making of this paper.

References

[1] **C C Adams**, *Thrice-punctured spheres in hyperbolic 3–manifolds*, Trans. Amer. Math. Soc. 287 (1985) 645–656 MR768730

[2] **C C Adams**, *Waist size for cusps in hyperbolic 3–manifolds*, Topology 41 (2002) 257–270 MR1876890

[3] **C C Adams**, *Noncompact Fuchsian and quasi-Fuchsian surfaces in hyperbolic 3–manifolds*, Algebr. Geom. Topol. 7 (2007) 565–582 MR2308957

[4] **I R Aitchison**, **E Lumsden**, **J H Rubinstein**, *Cusp structures of alternating links*, Invent. Math. 109 (1992) 473–494 MR1176199

[5] **L Bers**, *Quasiconformal mappings and Teichmüller's theorem*, from: "Analytic functions", Princeton Mathematical Series 24, Princeton Univ. Press (1960) 89–119 MR0114898

[6] **R D Canary**, **D McCullough**, *Homotopy equivalences of 3–manifolds and deformation theory of Kleinian groups*, Mem. Amer. Math. Soc. 812, Amer. Math. Soc. (2004) MR2096234

[7] **J H Conway**, *An enumeration of knots and links, and some of their algebraic properties*, from: "Computational problems in abstract algebra", (J Leech, editor), Pergamon, Oxford (1970) 329–358 MR0258014

[8] **D B A Epstein**, **R C Penner**, *Euclidean decompositions of noncompact hyperbolic manifolds*, J. Differential Geom. 27 (1988) 67–80 MR918457

[9] **S Francaviglia**, *Hyperbolic volume of representations of fundamental groups of cusped 3–manifolds*, Int. Math. Res. Not. 2004 (2004) 425–459 MR2040346

[10] **D Futer**, **E Kalfagianni**, **J Purcell**, *Quasifuchsian state surfaces*, to appear in Trans. Amer. Math. Soc. (2012)

[11] **W B R Lickorish**, *Prime knots and tangles*, Trans. Amer. Math. Soc. 267 (1981) 321–332 MR621991

[12] **A Marden**, *Geometrically finite Kleinian groups and their deformation spaces*, from: "Discrete groups and automorphic functions", (W J Harvey, editor), Academic Press, London (1977) 259–293 MR0494117

[13] **W Menasco**, *Closed incompressible surfaces in alternating knot and link complements*, Topology 23 (1984) 37–44 MR721450

[14] **W Menasco**, **M Thistlethwaite**, *The classification of alternating links*, Ann. of Math. 138 (1993) 113–171 MR1230928

[15] **J W Morgan**, *On Thurston's uniformization theorem for three-dimensional manifolds*, from: "The Smith conjecture", (J W Morgan, H Bass, editors), Pure Appl. Math. 112, Academic Press, Orlando, FL (1984) 37–125 MR758464

[16] **D Rolfsen**, *Knots and links*, Mathematics Lecture Series 7, Publish or Perish, Houston, TX (1990) MR1277811

[17] **D Ruberman**, *Mutation and volumes of knots in S^3*, Invent. Math. 90 (1987) 189–215 MR906585

[18] **M Sakuma**, **J Weeks**, *Examples of canonical decompositions of hyperbolic link complements*, Japan. J. Math. 21 (1995) 393–439 MR1364387

Department of Mathematics, University of Tennessee
Knoxville, TN 37996, USA

Department of Mathematics, University of California, Davis
One Shields Avenue, Davis, CA 95616, USA

morwen@math.utk.edu, n.tsvet@gmail.com

www.math.utk.edu/~morwen, www.math.ucdavis.edu/~tsvietkova

Received: 1 August 2011 Revised: 9 September 2013